

1 Title

2

3 **Eddy Covariance Evaluation of Ecosystem Fluxes at a Temperate Saltmarsh in**

4 **Victoria, Australia Shows Large CO₂ Uptake**

5

6 Authors

7

8 Ruth Reef¹,

9 Edoardo Daly^{2,3},

10 Tivanka Anandappa¹,

11 Eboni-Jane Vienna-Hallam¹,

12 Harriet Robertson¹,

13 Matthew Peck¹,

14 Adrien Guyot^{4,5}

15

16 Affiliations

17

18 1 School of Earth, Atmosphere and Environment, Monash University, VIC 3800, Australia

19 2 Department of Civil Engineering, Monash University, VIC 3800, Australia

20 3 WMAwater, Brisbane, QLD 4000, Australia

21 4 Atmospheric Observations Research Group, The University of Queensland, Brisbane,

22 Australia

23 5 Australian Bureau of Meteorology, Melbourne, Australia

24

25 Corresponding Author

26

27 Associate Professor Ruth Reef

28 School of Earth Atmosphere and Environment

29 Monash University

30 9 Rainforest Walk, Clayton VIC 3800

31 Australia

32 Email: ruth.reef@monash.edu

33 Ph: +61 3 9905 8309

34

35

36 Key Points

37

38 This is the first study using eddy covariance to measure CO₂ fluxes at an Australian
39 temperate saltmarsh, revealing temperature and light limitations to CO₂ uptake.

40

41 CO₂ fluxes varied seasonally; growing season net ecosystem productivity was 10.54 g CO₂
42 m⁻² day⁻¹, dropping to 1.64 g CO₂ m⁻² day⁻¹ in winter.

43

44 Productivity at the French Island saltmarsh is high relative to global saltmarsh estimates but
45 below global mangrove averages.

46

47

48

49 Abstract

50

51 Recent studies highlight the important role of vegetated coastal ecosystems in atmospheric
52 carbon sequestration. Saltmarshes constitute 30% of these ecosystems globally and are the
53 primary intertidal coastal wetland habitat outside the tropics. Eddy covariance (EC) is the
54 main method for measuring biosphere-atmosphere fluxes, but its use in coastal environments
55 is rare. At an Australian temperate saltmarsh site on French Island, Victoria, we measured
56 CO₂ and water gas concentration gradients, temperature, wind speed and radiation. The
57 marsh was dominated by a dense cover of *Sarcocornia quinqueflora*. Fluxes were seasonal,
58 with minima in winter when vegetation is dormant. Net ecosystem productivity (NEP) during
59 the growing season averaged 10.54 g CO₂ m⁻² day⁻¹ decreasing to 1.64 g CO₂ m⁻² day⁻¹ in
60 the dormant period, yet the marsh remained a CO₂ sink due to some sempervirent species.

61 Ecosystem respiration rates were lower during the dormant period compared with the
62 growing season (1.00 vs 1.77 μmol CO₂ m⁻² s⁻¹) with a slight positive relationship with
63 temperature. During the growing season, fluxes were significantly influenced by light levels,
64 ambient temperatures and humidity with cool temperatures and cloud cover limiting NEP.

65 Ecosystem water use efficiency of 0.86 g C kg⁻¹ H₂O was similar to other C₃ intertidal
66 marshes and evapotranspiration averaged 2.48 mm day⁻¹ during the growing season.

67

68 EGUsphere Topics

69 Emissions, Marine and Freshwater Biogeosciences, Earth System Biogeosciences

70

71 Short Summary

72

73 Studies show that saltmarshes excel at capturing carbon from the atmosphere. In this study,
74 we measured CO₂ flux in an Australian temperate saltmarsh on French Island. The temperate
75 saltmarsh exhibited strong seasonality. During the warmer growing season, the saltmarsh
76 absorbed on average 10.5 grams of CO₂ from the atmosphere per m² daily. Even in winter,
77 when plants were dormant, it continued to be a CO₂ sink, albeit smaller. Cool temperatures
78 and high cloud cover inhibit carbon sequestration.

79

80

81

82

83 1. Introduction

84

85 Despite their relatively small global footprint of 54,650 km² (Mcowen et al., 2017), salt
86 marshes provide a range of ecosystem services, including shoreline protection (Shepard et al.,
87 2011), nutrient uptake, nursery grounds for fish populations (Whitfield, 2017) as well as
88 functioning as significant carbon sinks through CO₂ uptake and storage in their organic rich
89 sediments (McLeod et al., 2011). These ‘blue carbon’ habitats are recognised for their
90 significant contribution to the global carbon cycle, as coastal wetlands more broadly are
91 estimated to have accumulated more than a quarter of global organic soil carbon (Duarte,
92 2017).

93

94 Saltmarshes are a widely distributed intertidal habitat but are floristically divergent globally
95 (Adam, 2002), such that commonalities in function and form do not extend across
96 biogeographic realms. US saltmarshes, for example, are extensively dominated by a single
97 grassy species, *Spartina alterniflora*, as opposed to the dominance of C₃ Chenopodioideae
98 species in the southern hemisphere (Adam, 2002). Temperate saltmarshes occupy a
99 latitudinal range spanning from approximately 30° to 60° (Mcowen et al., 2017) and are most
100 commonly found along protected coastlines such as bays, estuaries, and lagoons, where they
101 are sheltered from the full force of wave action (Mitsch and Gosselink, 2000). In the
102 Southern Hemisphere, temperate saltmarshes have a strong Gondwanan element with high
103 floristic similarity among the marshes of New Zealand, the southernmost coasts of South
104 America and South Africa and the southern coastlines of Australia (Adam, 1990). These
105 marshes are often associated with extensive seagrass meadows and mudflats, and in parts of
106 their range, mangroves, forming complex coastal mosaics (Huxham et al., 2018).
107 Saltmarshes have been heavily degraded across their range, and it is estimated that perhaps
108 up to 50% of the global saltmarsh area has been lost since 1900 (Gedan et al., 2009),
109 primarily due to land use change.

110

111 In most areas where they occur, seasonality plays a major role in the functioning of temperate
112 saltmarshes (Ghosh and Mishra, 2017). These ecosystems experience distinct growing and
113 dormant seasons, primarily driven by temperature, light availability, and precipitation
114 patterns (Adam, 2000). During the growing season (typically spring and summer), increased
115 temperatures and longer daylight hours stimulate plant growth, photosynthetic activity, and

116 decomposition processes. Photosynthesis typically outpaces decomposition during this
117 period, resulting in the temperate saltmarsh acting as a net CO₂ sink (Chmura et al., 2003).
118 Conversely, the dormant season (usually fall and winter) is characterized by cooler
119 temperatures and shorter days (Adam, 2000; Howe et al., 2010). These factors lead to
120 reduced plant growth and photosynthetic activity (Adam, 2000) and while decomposition
121 processes also slow down due to cooler temperatures, CO₂ release through decomposition
122 often exceeds CO₂ uptake during this period (Artigas et al., 2015). In Australia, saltmarshes
123 have been assumed to not exhibit seasonality (Owers et al., 2018) despite there being a
124 scarcity of data on saltmarsh phenology and the implication this untested assumption could
125 have on carbon budget estimations.

126
127 Gross primary production (GPP) of saltmarshes is the total amount of CO₂ uptake by plants
128 through photosynthesis. Respiration (R_c) leads to a CO₂ flux directed back to the atmosphere
129 due to all respiration processes occurring within the saltmarsh, involving both autotrophs and
130 heterotrophs. The difference between these two fluxes is the net ecosystem exchange (NEE).
131 Saltmarsh ecosystems can act as both sources and sinks of carbon dioxide (CO₂), influencing
132 atmospheric CO₂ concentrations (Chmura et al., 2003). However, quantifying their net
133 exchange remains challenging (Lu et al., 2017) hindering their effective inclusion in Earth
134 System Models (Ward et al., 2020) and confounding the incorporation of saltmarsh
135 restoration in emission reduction targets. Eddy covariance (EC) provides a powerful method
136 for near-continuous, high-frequency monitoring of gas exchange between a vegetated surface
137 and the atmosphere (Baldocchi, 2003), enabling the determination of net ecosystem exchange
138 (NEE) of CO₂, and identifying the forcings that determine how CO₂ fluxes will respond to
139 global climate change (Borges et al., 2006; Cai, 2011).

140
141 Previous EC studies in coastal saltmarshes have been focused on the Northern Hemisphere, in
142 sites in the USA (e.g. Hill and Vargas, 2022; Kathilankal et al., 2008; Moffett et al., 2010;
143 Nahrawi et al., 2020; Schäfer et al., 2019), France (Mayen et al., 2024), Japan (Otani and
144 Endo, 2019) and China (Wei et al., 2020) but interest in the southern hemisphere is growing
145 (Bautista et al., 2023). The NEE values from these studies indicate that there is high inter-site
146 (as well as interannual, Erickson et al., (2013)) variability in carbon dynamics of saltmarshes,
147 with a link to species types, salinity, hydrology (Moffett et al., 2010; Nahrawi et al., 2020),
148 site specific biochemical conditions (Seyfferth et al., 2020) and latitude (Feagin et al., 2020).
149 While generally considered important carbon sinks (e.g. ranging between 130 to 775 g C m⁻²

150 yr⁻¹ in the USA, according to Kathilankal et al. (2008) and Wang et al.(2016) respectively)
151 and globally hypothesised to average 382 g C m⁻² y⁻¹ (Alongi, 2020), some EC studies
152 revealed saltmarshes to be net sources of CO₂ to the atmosphere (Vázquez-Lule and Vargas,
153 2021) especially in temperate saltmarshes that experience long dormant periods.

154

155 The aim of this study is to estimate CO₂ and water fluxes in a temperate saltmarsh in
156 Victoria, southern Australia, to better characterise the effect of seasonality and environmental
157 variables on the saltmarsh CO₂ budgets. This is the first study in an Australian coastal
158 saltmarsh where CO₂ fluxes are estimated using the EC method.

159

160 2. Methods

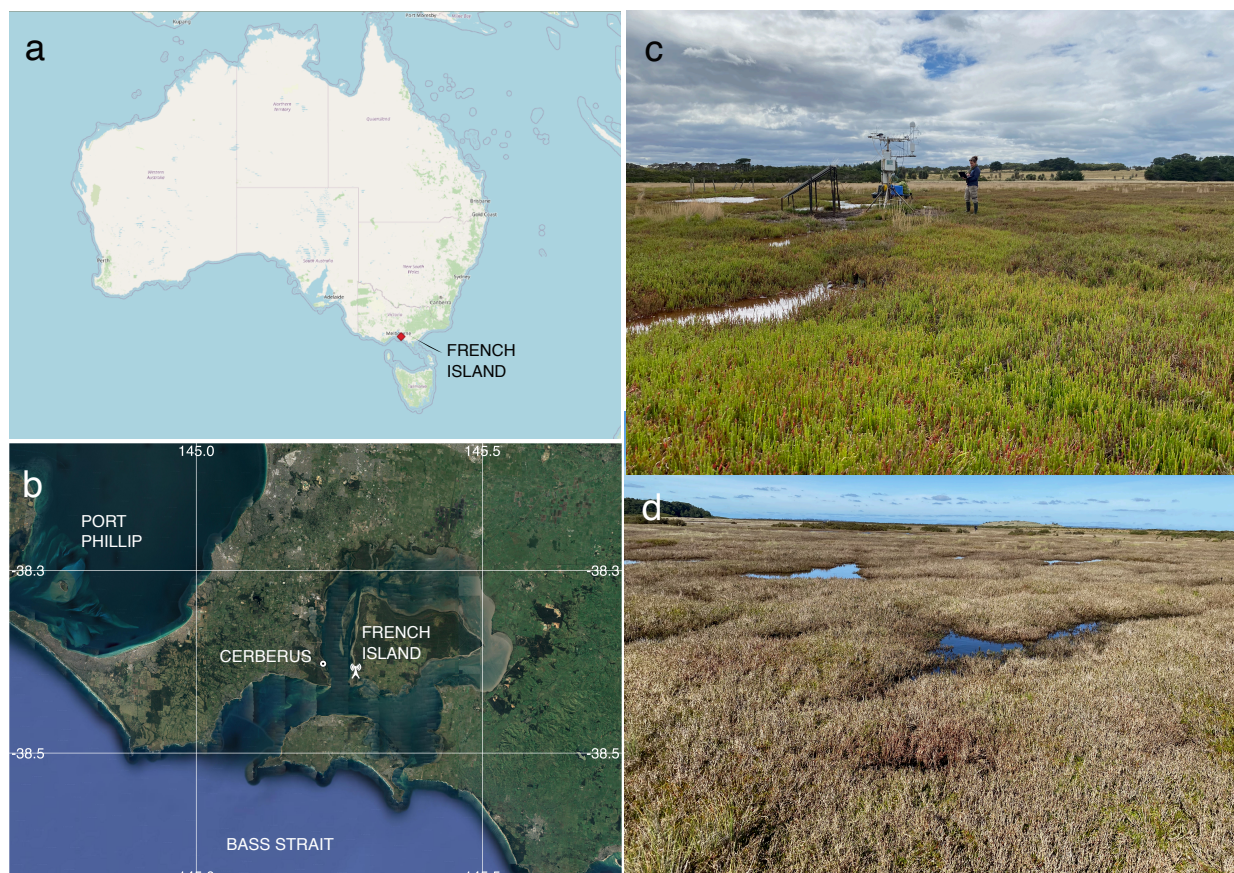
161

162 2.82 Site Description

163

164 Ecosystem flux measurements were collected at the Tortoise Head Ramsar coastal wetland on
165 French Island, Victoria (38.388°S, 145.278°E, Fig. 1) within the Western Port embayment.
166 French Island is within the Cfb climate zone (temperate oceanic climate) and experiences
167 distinct seasonal variations in temperature and precipitation. Long term (30 year) climate data
168 averaged from the nearby Cerberus Station (Australian Bureau of Meteorology, site 86361)
169 indicated that summers, spanning from December through February, are generally mild to
170 warm, with maximum temperatures typically ranging from 17°C to 25°C although occasional
171 heatwaves lead to temporary spikes in temperature that can exceed 30°C. Winters, from June
172 to September, are cooler, with maximum temperatures ranging between 7°C and 14°C and a
173 mean minimum temperature of 6°C. Frost is infrequent due to maritime influence, though
174 crisp mornings below 0°C occur 10% of the time in winter. Rainfall, evenly distributed
175 throughout the year, averages ca. 715 mm y⁻¹, although in 2020 the site Ied higher than
176 average rainfall (860 mm y⁻¹). The island is exposed to weather patterns influenced by the
177 Southern Ocean and Bass Strait, leading to occasional storm systems, particularly in winter,
178 bringing gusty winds and increased precipitation. Western Port has semi-diurnal tides with a
179 range of nearly 3 m, resulting in wide intertidal flats occupied by mangroves of the species
180 *Avicennia marina* and saltmarshes.

181



182
183

184 Figure 1: a) The location of French Island along the Bass Strait coast of Australia, and b) The
185 location of the flux tower on French Island as well as the nearby Cerberus meteorological
186 station (Bureau of Meteorology, Australia), © Google Earth. c) An image of the saltmarsh
187 within the flux tower footprint during the growing season (with the tower and the author in
188 the background), taken in February 2020 by Prudence Perry. d) an image of the saltmarsh
189 during the dormant period, taken at the same location in September 2020 by Ruth Reef.

190

191 The site at French Island is dominated by an extensive temperate coastal saltmarsh
192 community that is a particularly good natural representation of a broader biogeographic
193 saltmarsh grouping which covers an area of ca. 7000 ha along Victoria's central coast
194 embayments (Navarro et al., 2021). While the wetland at the site is a saltmarsh-mangrove-
195 seagrass wetland system, the footprint of the flux tower was limited to the saltmarsh alone,
196 which extends more than a kilometre from the shoreline in places. This geography provided
197 the critical horizontally homogenous area with flat terrain required for ecosystem flux
198 measurements. Floristically this saltmarsh is species poor, dominated by *Sarcocornia*
199 *quinqueflora*. Stands of *Tecticornia arbuscula* are common in this saltmarsh, while *Atriplex*
200 *cinerea* approx. 7% and *Distichis distichophylla* can be prevalent depending on

201 elevation and soil drainage conditions. *Sarcocornia quinqueflora* is a perennial succulent and
202 at the temperate ranges of its distribution it has a distinct growing season from October to
203 May (Fig. 1c) when the stems turn red, followed by a woody and fibrous dormant period
204 during the colder months of June through September (Fig. 1d). The height of the dominant
205 vegetation ranged between 0.3 m.

206

207 2.83 2.2 Data Collection and Analysis

208

209 Eddy covariance measurements were made between November 2019 and August 2021
210 capturing both the saltmarsh growing season (October-May) as well as a dormant period
211 (June-September). An array of standard micro-meteorological instruments included a 3-
212 dimensional sonic anemometer (CSAT3, Campbell Scientific, USA), an open-path infra-red
213 carbon dioxide (CO₂) gas and water vapour (H₂O) analyser (Li-7500, Li-Cor, USA) and 2
214 data-loggers. The tower was powered by a solar array with two accompanying 12V DC
215 storage batteries. The sonic anemometer was mounted 2.3 m above ground. The CO₂/H₂O
216 gas analyser was mounted 0.11 m longitudinally displaced from the anemometer. A CR3000
217 datalogger (Campbell Scientific, USA), recorded the Li-7500, anemometer, short- and long-
218 wave radiation (CNR4, Klip & Zonen, the Netherlands), air temperature and humidity (083E,
219 Met One, USA) readings at 10 Hz frequency. Due to the location of the site in the Bass Strait
220 (a region that experiences regular winter storms, high wind speeds and higher than national
221 average cloud cover) the tower sustained damage due to winter storms several times during
222 the deployment, as well as suffered periods of poor power supply due to short day lengths
223 and high cloud cover; this was exacerbated by poor accessibility to the remote location during
224 COVID-19 travel restrictions. The analysis thus focused on extended periods of continuous
225 daily records and periods with large gaps in the dataset were removed.

226

227 Ecosystem fluxes were calculated for 30 min intervals using Eddy Pro software v.7 (LI-COR
228 Inc., USA) Express Mode protocols. This processing step includes coordinate axis rotation
229 correction, trend correction, data synchronisation, statistical tests for quality, density
230 corrections and spectrum corrections. As part of this step, flux quality flags were assigned to
231 the calculated CO₂ fluxes using the 0–2 flag policy ‘Mauder and Foken 2004’, based on the
232 steady state test and the developed turbulent conditions test. The steady state test checks if
233 fluxes remain consistent over the 30-minute averaging period by comparing the mean and

234 standard deviation (SD) of fluxes in the first and second halves of the period. The developed
 235 turbulent conditions test ensures turbulence is well-developed and its energy spectra fits the
 236 Kolmogorov spectrum. Both tests assign partial flags that are combined into a single flag (0–
 237 2) in Eddy Pro, indicating the overall data quality. Only data that met the criteria of being in
 238 quality class 0 ('best quality fluxes') for CO₂ flux were chosen for further analysis. We
 239 further removed anomalous data points defined as values that exceed four SDs from the mean
 240 CO₂ flux; this resulted in the additional loss of ca. 1% of the dataset. Gap filling was not
 241 applied. Additional filtering was applied to nighttime data due to known weak convection at
 242 night, thus CO₂ flux data during periods of atmospheric stability, i.e. when night friction wind
 243 velocities (u^*) were below 0.2 m s⁻¹, were excluded following inspection of the nightly NEE
 244 vs. u^* curve to detect the threshold where NEE fall-off occurs. 0.2 m s⁻¹ is the typical
 245 threshold value used in eddy-covariance studies (Davis et al., 2003). This resulted in a dataset
 246 of 674 day-time and 606 nighttime flux measurements during the dormant period and 4124
 247 day-time and 3020 nighttime flux measurements for the growing period (Table 1). The
 248 growing season dataset included 90 days with 85% or more flux data coverage, while the
 249 dormant season dataset included 18 days, and these days were used for 24-hour flux
 250 integrations.

251

252 Table 1: Mean (\pm SD) net ecosystem exchange ($\mu\text{mol CO}_2 \text{ m}^{-2} \text{ s}^{-1}$) during day- and nighttime
 253 respectively, as well as the corresponding number of half hourly measurements from each
 254 month, following filter applications (n). Pink shading indicates the dormant season at the
 255 French Island saltmarsh.

256

Month	Daytime Mean NEE (SD); n	Nighttime Mean NEE (SD); n
October 2019	-2.29 (3.08); 121	2.04 (1.28); 70
November 2019	-1.84 (3.89); 151	2.85 (1.75); 110
December 2019	-3.33 (4.59); 96	1.14 (1.70); 15
January 2020	-1.31 (3.31); 63	2.10 (0.79); 27
February 2020	-3.83 (4.11); 540	1.89 (1.10); 280
March 2020	-3.86 (3.90); 494	1.63 (0.78); 351
August 2020	0.05 (2.05); 150	1.76 (1.22); 39
September 2020	-0.98 (2.04); 147	1.27 (0.96); 101
January 2021	-4.81 (5.04); 602	2.15 (1.55); 373
February 2021	-3.62 (4.27); 615	2.00 (1.19); 423
March 2021	-3.07 (3.95); 660	1.76 (1.20); 556
April 2021	-2.08 (3.02); 409	1.15 (0.87); 403

May 2021	-0.98 (2.57); 377	1.14 (1.04); 423
June 2021	0.58 (1.67); 271	0.93 (1.30); 328
July 2021	1.07 (1.38); 102	0.82 (0.62); 127

257

258

259 Half-hourly average CO₂ flux was measured in $\mu\text{mol m}^{-2} \text{s}^{-1}$, with positive fluxes indicating a
 260 flux direction from the Earth's surface to the atmosphere. Net ecosystem exchange (NEE)
 261 was defined as the net flux of CO₂ from the atmosphere to the marsh and was often negative
 262 during daytime, indicating that Gross Primary Productivity (GPP) was larger than ecosystem
 263 respiration (R_e). Evapotranspiration (ET) was calculated by Eddy Pro as the ratio between the
 264 latent heat flux (LE) and latent heat of vaporisation (λ). Ecosystem water use efficiency
 265 (WUE_e) was then expressed as the ratio between daytime net ecosystem productivity in g
 266 CO₂ m⁻² h⁻¹ and evapotranspiration in mm h⁻¹.

267

268 A two-dimensional footprint estimation was provided according to the simple footprint
 269 parameterisation described in Kljun et al. (2015) calculating the ground position of the
 270 cumulative fraction of flux source contribution by distance for each 30-minute interval. We
 271 assessed the short-term effects of environmental factors on CO₂ fluxes at a half-hourly time
 272 scale (e.g. the effects of light, air temperature and vapour pressure deficit) using a series of
 273 non-linear or linear models. These analyses were limited to the growing season, when the
 274 plants were actively photosynthesising. To calculate the daily-integrated CO₂ and H₂O fluxes,
 275 the daily sum of these fluxes was determined for days with at least 85% data coverage. This
 276 involved using the trapezoid rule to estimate the area under the curve for each of these 24-
 277 hour periods. The trapezoid rule approximates the total flux by dividing the day into smaller
 278 intervals, each lasting 1,800 seconds. For each interval, the area is calculated by averaging
 279 the flux values at the beginning and end of the interval, then multiplying by the interval
 280 duration. These areas are then summed to obtain the total daily flux. This method ensures that
 281 even with some missing data points, a reliable estimate of the daily flux can be obtained. All
 282 post-processing and statistical analyses were performed in R 4.3.2 (R Core Team, 2024)
 283 including the packages *ggplot2*, *clifro*, *MASS*, *dismo*, *amerifluxr*, *rmarkdown*, *geosphere*,
 284 *ggmap* and *gbm*.

285

286 Because of the large data gaps, it was not possible to model the partition of the NEE in GEP
 287 and R_e using common partitioning methods (Lasslop et al., 2010). For simplicity, it was

288 assumed that NEE at night coincided with R_e . R_e was corrected for temperature effects on
289 respiration using a linear slope of the relationship between nighttime NEE and temperature.
290 For the CO₂ budget, Net Ecosystem Production (NEP), was defined as $NEP = -NEE$.

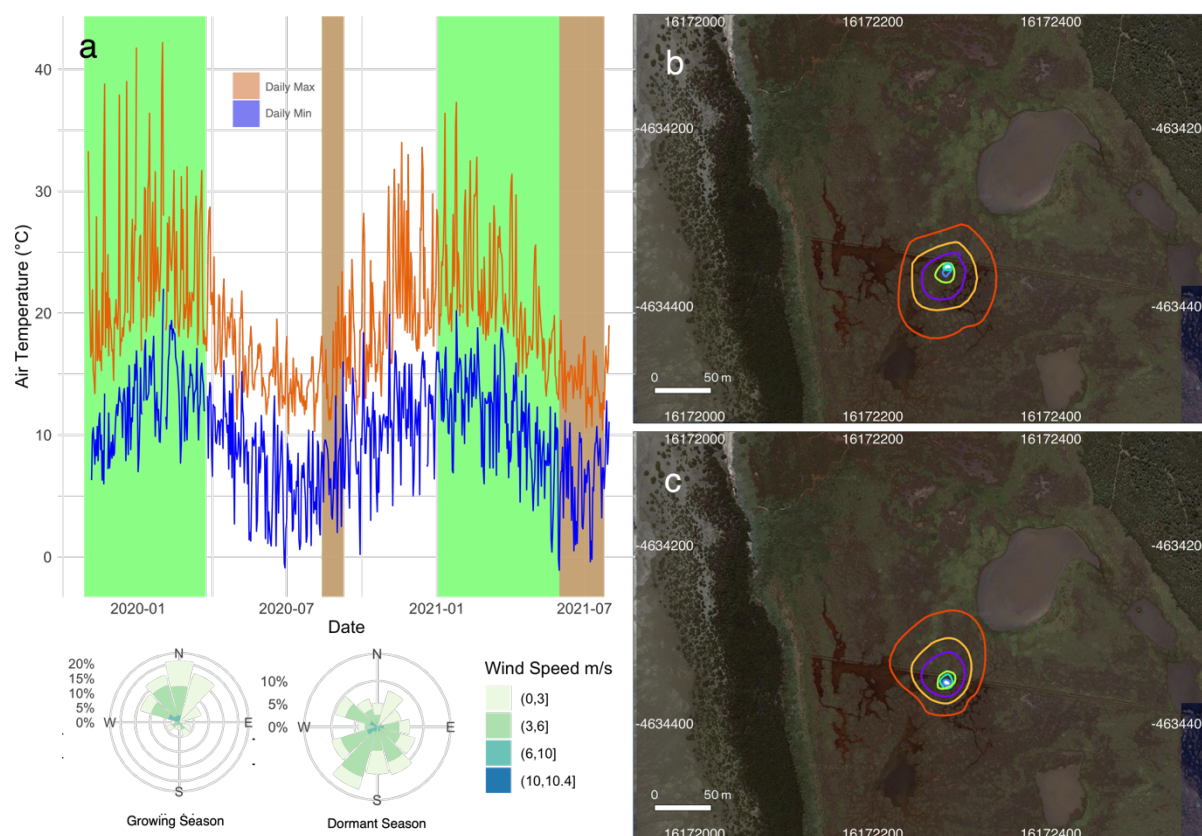
291

292 3. Results

293

294 The observations were divided into a growing season and a dormant season to reflect the
295 seasonal phenology of the dominant vegetation type within the flux tower footprint, which
296 has a relatively short growing season during the summer. During the growing season, mean
297 temperature averaged 22.3°C. Several heatwaves occurred during this period, with
298 temperatures exceeding 40°C on a few occasions in 2019. The dormant season was
299 significantly colder and windier, with frequent southerly winds (Fig. 2a). Footprint models
300 showed a slight variation in flux source between the two seasons, although in both cases the
301 size of the footprint and the vegetation composition within the footprint was similar (Figs. 2b
302 and 2c), but the shape was skewed to the north during winter due to the prevalent southerly
303 winds in that season (Fig. 2a). 70% of the flux measurement source was from within 50 m of
304 the tower, while the maximum length of the source location was 73 m.

305



306

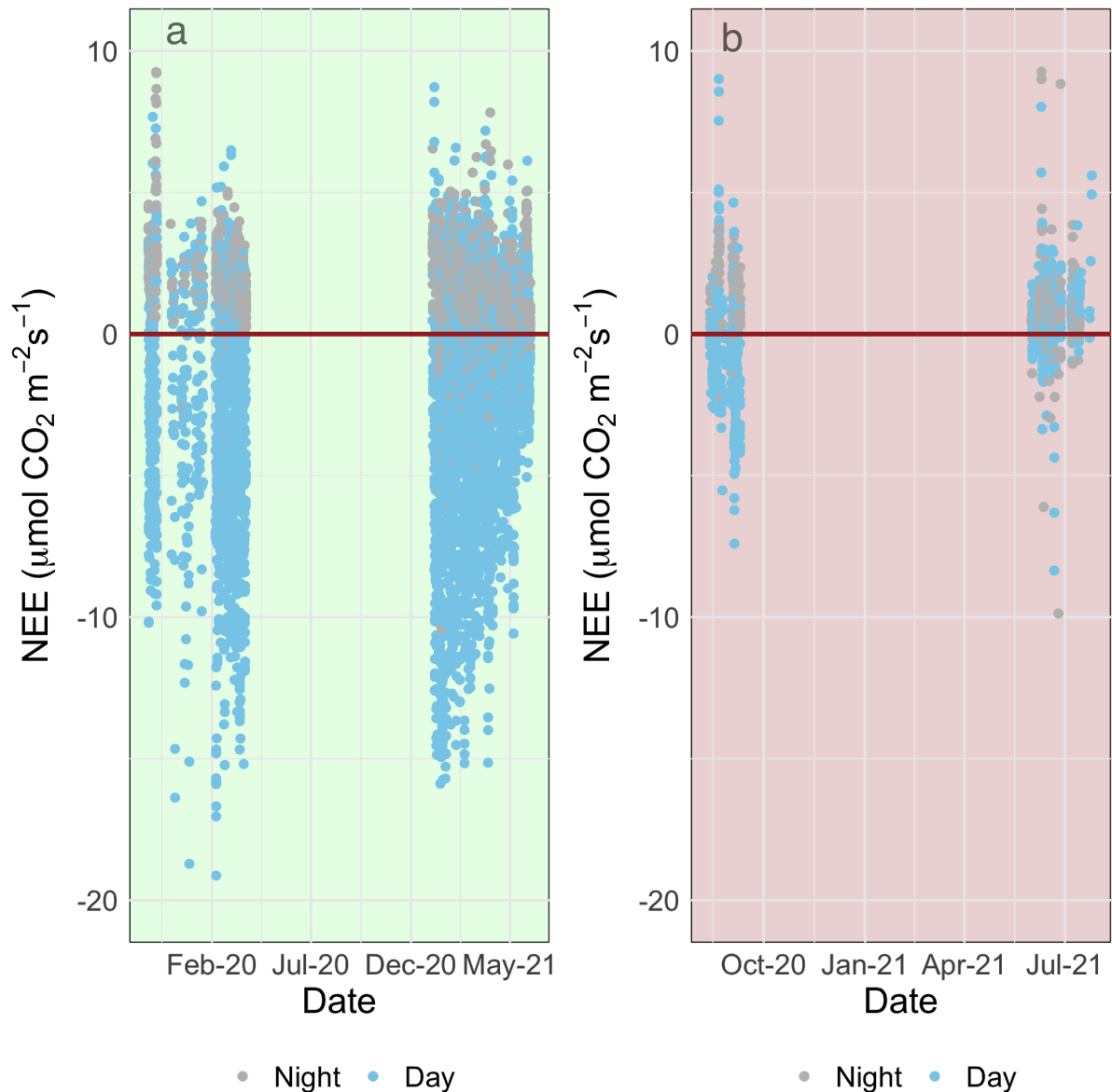
307

308 Figure 2: a) The minimum and maximum daily temperature recorded at the Cerberus
309 meteorological station (Bureau of Meteorology, Fig. 1b) during 2019-2021. The marsh
310 growing (October-May) and dormant (June-September) periods observed during this study
311 are shaded in green and pink respectively. A corresponding wind rose diagram summarises
312 the wind speeds and directions measured at the tower site during the observation periods. The
313 flux source footprint surrounding the tower during the dormant season (b) and the growing
314 season (c) shows the cumulative flux source contribution to the flux measurements, with the
315 outer red line representing the distance by which 90% of the calculated flux is sourced and
316 the other isolines from the tower outwards correspond to 10%, 20%, 40%, 60% and 80% of
317 the flux.

318

319 The growing season dataset included 90 days with 85% or more flux data coverage, while the
320 dormant season dataset included 18 days. There was a strong temporal variability in net
321 ecosystem exchange (NEE) across both short (daily) and long (seasonal) temporal scales
322 (Fig. 3). Daytime fluxes were defined as flux points where the global radiation values in the
323 flux averaging half-hour interval were $>12 \text{ W m}^{-2}$ (as per EddyPro methodology). At the
324 diurnal scale, saltmarsh NEE were negative mostly during the day and positive mostly during
325 the night and ranged between -19.1 and $10.86 \mu\text{mol m}^{-2} \text{ s}^{-1}$ across the measurement periods.
326 Monthly averages and data coverage are shown in Table 1.

327



328

329

330 Figure 3: A time series of half-hourly measurements of CO₂ flux between a temperate
 331 saltmarsh and the atmosphere measured by eddy covariance during the marsh growing season
 332 (a) and the dormant season (b). Blue and grey points indicate measurements taken during
 333 daytime and nighttime respectively. Positive fluxes indicate a direction of flux from the Earth
 334 surface to the atmosphere.

335

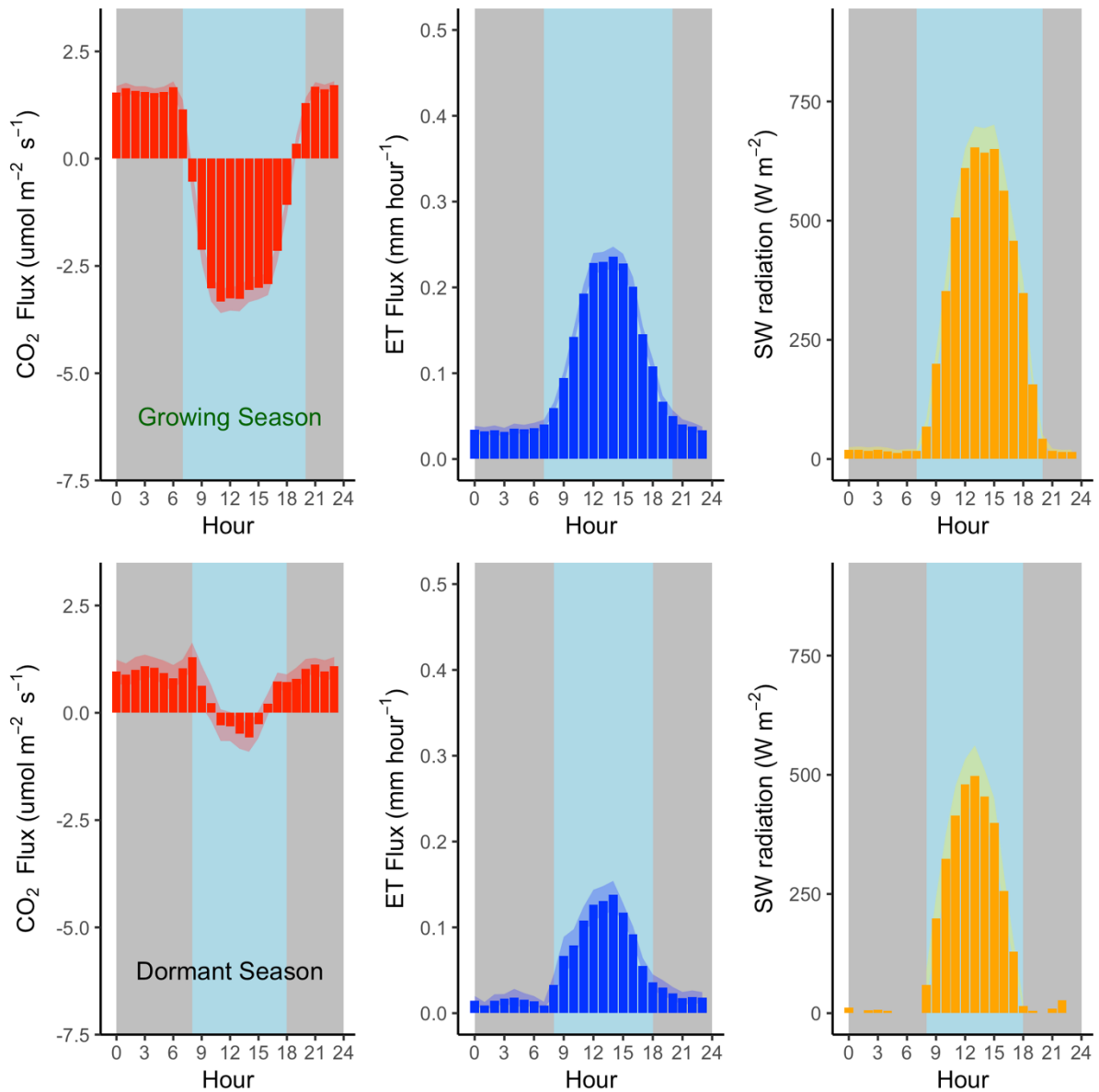
336 Flux rates varied across the day, with CO₂ uptake peaking at 11:00 during the growing
 337 season, and later in the day (14:00) during the dormant period (Fig. 4). Ecosystem respiration
 338 rates (R_e , defined as nighttime CO₂ flux) were on average (\pm SD) 1.77 (\pm 1.12) $\mu\text{mol m}^{-2} \text{s}^{-1}$
 339 during the growing season and 1.0 (\pm 0.93) $\mu\text{mol m}^{-2} \text{s}^{-1}$ during the dormant period. The

340 difference in ecosystem respiration between the growing and dormant seasons is highly
341 significant (t-test, $p < 0.01$). Daytime CO_2 flux was on average (\pm SD) $-3.53 (\pm 4.15) \mu\text{mol m}^{-2}$
342 s^{-1} during the growing season and $-0.25 (\pm 2.18) \mu\text{mol m}^{-2} \text{s}^{-1}$ during the dormant season.
343 Thus, we derive that the maximum Gross Primary Productivity (GPP) of this ecosystem from
344 NEE and temperature-corrected R_e (Fig. 5), measured during the growing season, is ca. -5.34
345 $\pm 4.3 \mu\text{mol CO}_2 \text{ m}^{-2} \text{ s}^{-1}$ ($-5.53 \pm 4.45 \text{ g C m}^{-2} \text{ day}^{-1}$). Average R_e is thus estimated to comprise
346 33% of GPP.

347

348 Mean (\pm SD) daily evapotranspiration was $2.48 \text{ mm} (\pm 2.79 \text{ mm})$ during the growing season
349 and $0.97 \text{ mm} (\pm 1.35 \text{ mm})$ during the dormant season (Fig. 4). Evapotranspiration peaked at
350 noon AEST during the growing season (0.26 mm h^{-1}), and later in the day (14:00 AEST)
351 during the dormant season (0.14 mm h^{-1}).

352



353

354

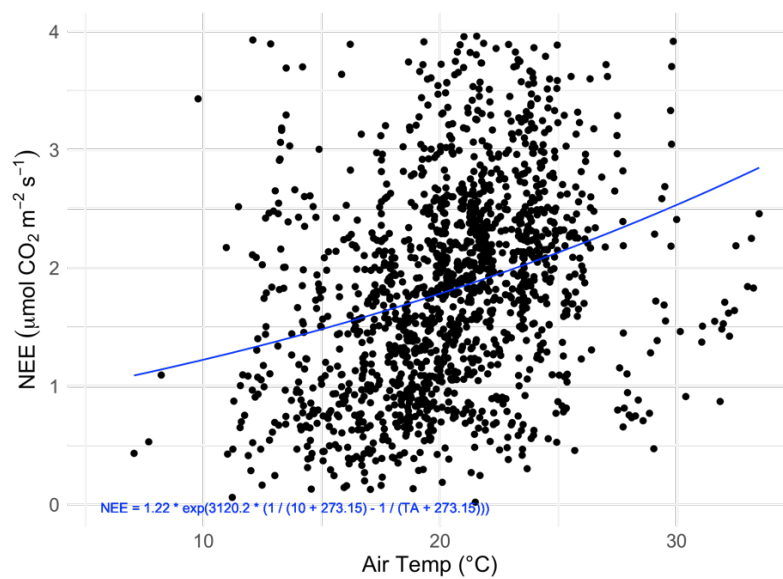
355 Figure 4: Mean hourly CO₂ and H₂O flux (evapotranspiration) rates during the growing
 356 season (top) and the dormant season (bottom) alongside mean short wave incoming radiation.

357 Shading corresponds to 1 standard deviation (SD) around the mean. Grey plot background

358 approximates nighttime periods, while light blue approximates daytime (actual day length

359 varies within each season).

360



361

362 Figure 5: The relationship between nighttime half-hourly flux measurements (NEE) taken
 363 between the hours of 22:00 and 02:00 and air temperature (TA). The fitted curve (blue line) is
 364 the fitted Lloyd & Taylor Arrhenius non-linear model: $NEE = 1.22 * \exp(3120.2 * (1/283.2 -$
 365 $1/(TA+273.2)))$, $R^2 = 0.09$.

366

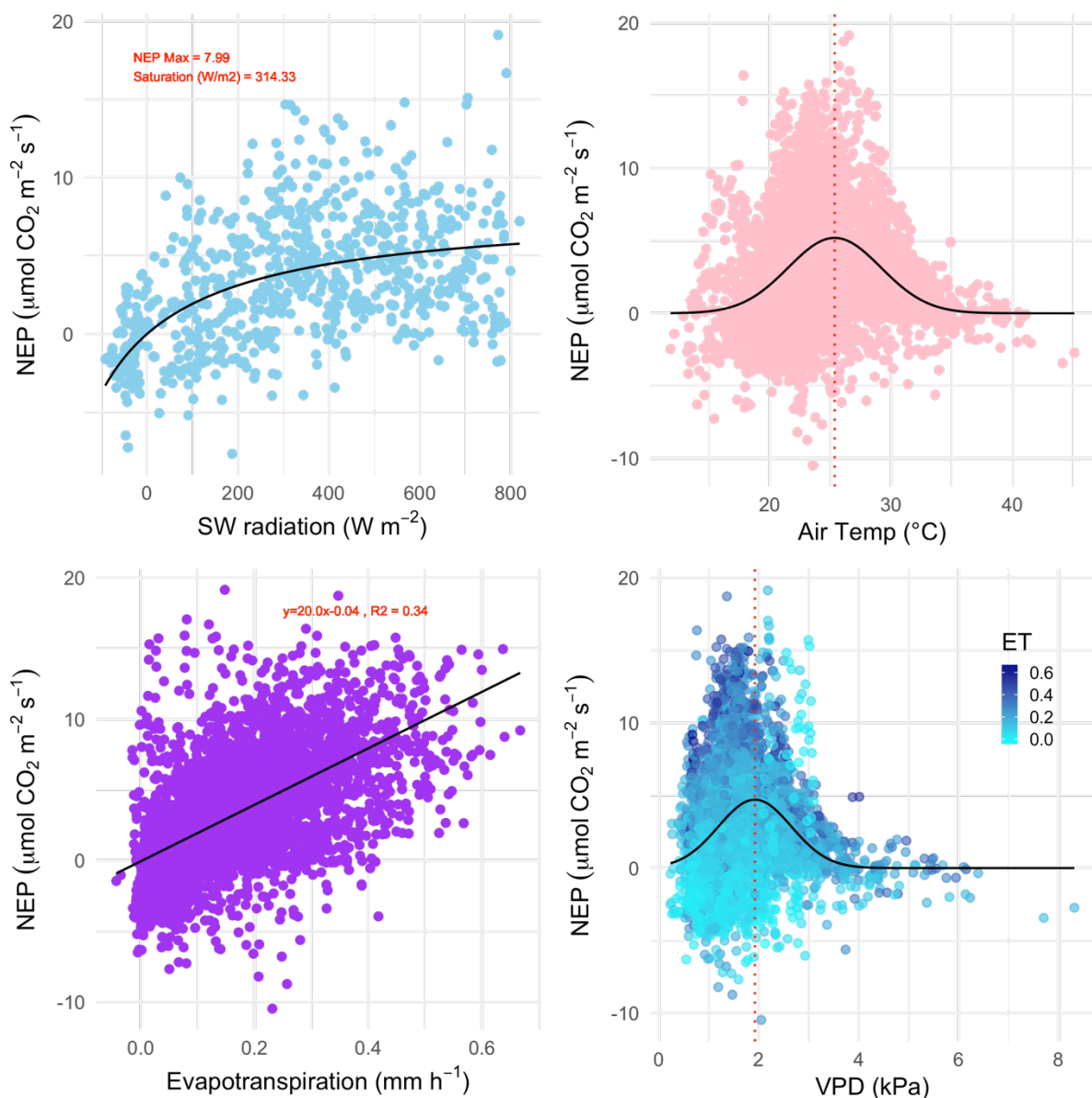
367 The effect of some environmental forcings on daytime NEE during the saltmarsh growing
 368 season were explored (Fig. 6). To distinguish this daytime-only value from the 24-hour
 369 carbon balance integration, and to better highlight CO₂ uptake, NEP values are shown.

370

371 Short wave radiation (visible light) was a limiting factor to NEP below approximately 300 W
 372 m⁻², but radiation did not reach damaging levels that would lead to a drop in NEP throughout
 373 the measurement range, which reached a maximum level of ca. 800 W m⁻². Unlike light, the
 374 NEP-air temperature relationship followed a Gaussian response, with the highest NEP
 375 achieved at the optimal temperature of 25.3°C with a SD of 3.8°C followed by a decline in
 376 CO₂ uptake by the marsh at higher temperatures. The minimum and maximum air
 377 temperatures for which modelled NEP nears zero (defined here as 3 SDs from the mean) are
 378 13.9°C and 36.7°C respectively. Temperature also had a slight but significant positive linear
 379 relationship with ecosystem respiration (slope=0.07 μmol CO₂ m⁻² s⁻¹ °C⁻¹, p<0.01, data not
 380 shown).

381

382 NEP was positively correlated with evapotranspiration during the growing season (Pearson r
 383 = 0.59, Fig.6 C). The slope of the NEP/ET relationship was 20.0, indicating an ecosystem
 384 water use efficiency (WUE_e) of 0.86 g C kg⁻¹ H₂O ($R^2 = 0.34$, $p < 0.001$). The response of
 385 NEP to atmospheric vapour pressure deficit (VPD) fit a Gaussian relationship (the commonly
 386 observed inverse U-shaped curve relationship in response to VPD in plants), with NEP
 387 declining rapidly when VPD exceeded 2.39 kPa. The optimal range of VPD within which
 388 NEP was maximised in this ecosystem was 1.92 kPa (± 0.73 kPa).
 389



390
 391 Figure 6: The relationship between growing season daytime half-hourly values of net
 392 ecosystem productivity (NEP, $\mu\text{mol CO}_2 \text{ m}^{-2} \text{ s}^{-1}$) and corresponding environmental variables.
 393 a) Net shortwave (SW) radiation (visible light); black line is the Michaelis-Menten model of

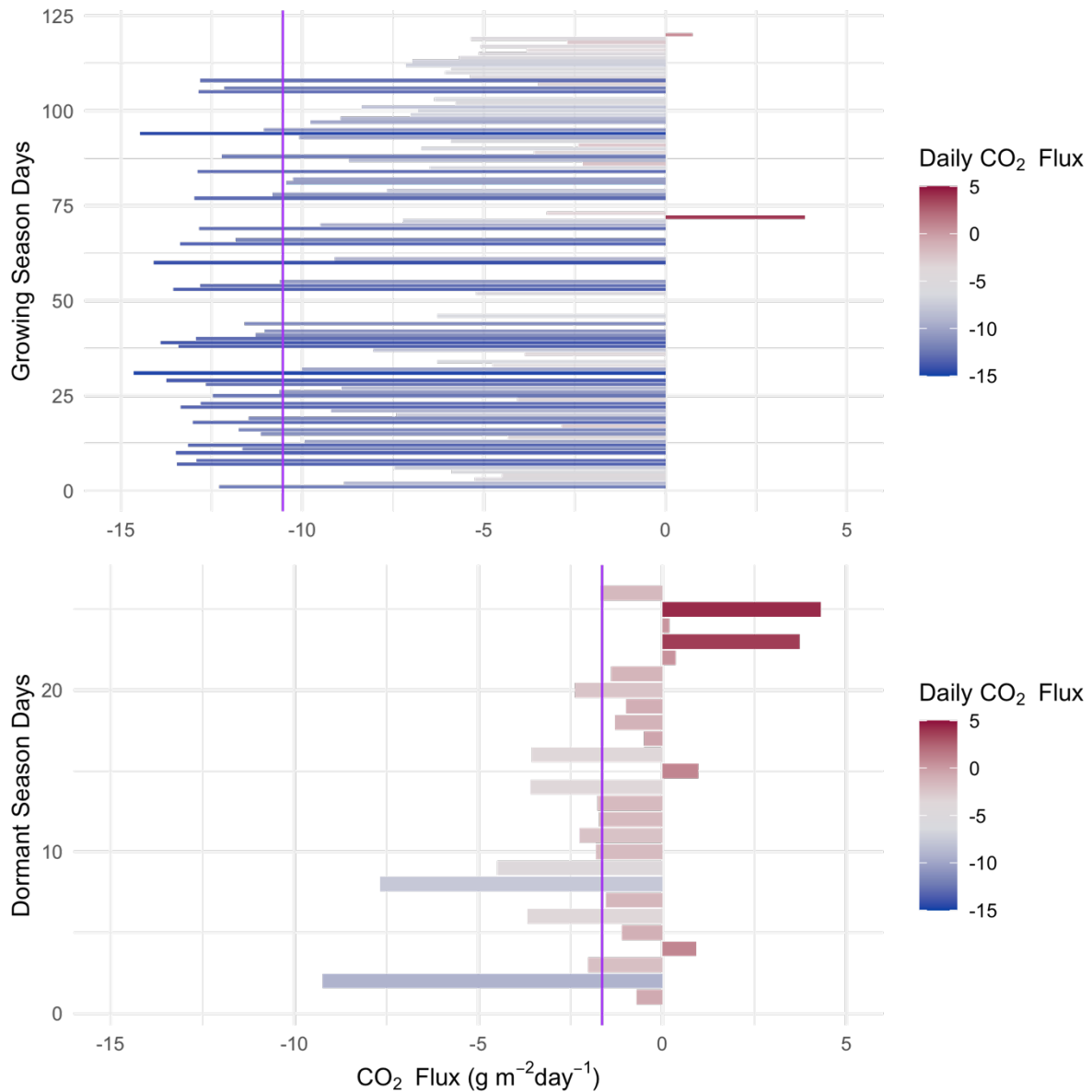
394 best fit. The coefficient of saturation is at 314 W m^{-2} and maximum net productivity is 8.0
395 $\mu\text{mol CO}_2 \text{ m}^{-2} \text{ s}^{-1}$. b) Air temperature; black line is a Gaussian model of best fit with a
396 temperature optimum at 25.3°C . c) Evapotranspiration; linear model ($R^2 = 0.34$) has a slope
397 of 20.0 . d) Vapour Pressure Deficit; black line is a Gaussian model of best fit with a VPD
398 optimum at 1.92 kPa , points are coloured by the level of evapotranspiration during the half
399 hourly NEP measurement.

400

401 When integrated over a 24-hour period, the saltmarsh is on average a daily CO_2 sink during
402 all canopy phenological phases (Fig. 7), although during the dormant season the sink is
403 weaker, with an average uptake of $-2.42 \text{ g CO}_2 \text{ m}^{-2} \text{ day}^{-1}$ (± 2.54). During the growing season
404 (defined as the non-dormant period and thus reflecting several phenological stages), the
405 marsh is a substantial sink with a mean ($\pm\text{SD}$) daily NEP of $10.95 \text{ g CO}_2 \text{ m}^{-2} \text{ day}^{-1}$ (± 4.98)
406 over a 24-hour period (ranging between -22.8 and $4.3 \text{ g of CO}_2 \text{ emission to the atmosphere}$
407 $\text{m}^{-2} \text{ day}^{-1}$). The daily CO_2 budget during the growing season showed some variability among
408 days ($\text{CV}=0.46$, Fig. 7) and days with lower average light levels (i.e. cloudy days) had a
409 significant negative impact on the CO_2 budget (multiple linear regression, $p < 0.02$, $R^2 =$
410 0.27). Daily maximum air temperatures did not have a significant impact on the daily CO_2
411 budget ($p = 0.77$) at this location, although NEE was significantly affected by temperature at
412 finer temporal scales (Figure 6).

413

414



415

416 Figure 7: Daily (24 h) integrated NEE in g CO₂ m⁻² day⁻¹ during the saltmarsh growing
 417 season (top) and the dormant season (bottom) for days with data density > 85%. Purple lines
 418 indicate the mean daily integrated flux for each season (-10.54 and -1.64 g CO₂ m⁻² day⁻¹ with
 419 an SD of 4.98 and 2.54 for growing and dormant respectively). A positive balance indicates
 420 an integrated net flux of CO₂ from the Earth's surface to the atmosphere over the 24-hour
 421 period.

422

423

424 4. Discussion

425

426 The study provided high-frequency measurements of an abundant greenhouse gas (CO₂)
427 using a precise technique (eddy covariance flux) in an ecosystem with limited historical
428 measurements. Time series analysis was performed on CO₂ flux measurements across various
429 scales (daily, nightly, diel, half-hourly, hourly, seasonally) to assess the impacts of ET, SW
430 Rad, VPD, and Tair on CO₂ flux and how these relationships change throughout the year.
431 Seasonality was observed for the first time in an Australian saltmarsh and had a significant
432 effect on carbon and water flux. Growing season net ecosystem productivity was five times
433 greater than during the dormant period. Seasonality in Australian marshes has not been
434 previously reported in the scientific literature and contradicts previous assumptions that
435 Australian saltmarshes do not exhibit the growing and dormant phenology observed on other
436 continents (Clarke and Jacoby, 1994). Seasonality had a significant impact on the carbon
437 budget in this marsh and is an important characteristic of this habitat that has been
438 overlooked (Owers et al., 2018). Seasonality can also have other broader implications yet to
439 be considered in Australian marshes. For example, in the USA, the saltmarsh greening up
440 period was shown to be an important range-wide timing event for migratory birds (Smith et
441 al., 2020) with plant-growth metrics predicting the timing of nest initiation for shorebirds.
442 Saltmarshes in Australia are important roosting and feeding sites along the East Asian
443 Australasian Flyway, particularly for waders, thus potentially a similar relationship between
444 migration timing and saltmarsh phenology could be occurring. Seasonality also affects other
445 significant ecosystem functions such as the bio-geomorphological feedback between
446 saltmarshes, coastal hydrodynamics and landscape evolution (Reents et al., 2022).

447
448 We derived the light-response and associated coefficients of light regulation of saltmarsh
449 NEE using the Michaelis Menten model (Chen et al., 2002). Quantum (or production)
450 efficiency is the predominant input in remote sensing techniques to model productivity, and is
451 specific to the biome (Hilker et al., 2010). While not directly comparable to leaf level
452 quantum efficiency measurements, the quantum efficiency (α) of the NEP light response
453 curve was estimated from the slope of the Michaelis-Menten model to be 0.025 $\mu\text{mol CO}_2 \text{ J}^{-1}$.
454 The ecosystem reached light saturation at an insolation of 314 W m^{-2} , but daytime insolation
455 was below this value more than 50% of the time suggesting that light might be a significant
456 limiting factor to NEP at this marsh, especially during winter. The level of light limitation we
457 observed is an underestimation, due to the loss of high-quality EC data during periods of rain.
458 The solar geometry at this latitude and the length of day result in an annual average top of

459 atmosphere SW radiation of 250 W m^{-2} , but clouds can strongly modulate the SW radiation
460 balance (SWCRE), and apart from the months of January and February when cloudy days are
461 less frequent (10-12 days per month), cloudy days are frequent at this site, averaging 15-17
462 days per month (Bureau of Meteorology) and could significantly impact on NEP.

463

464 Temperature is another forcing that significantly impacts NEE at this marsh, with an optimal
465 range for maximum NEP at 25.3°C (21.5°C - 29.1°C). Data for Australian saltmarshes is not
466 available, but this optimal temperature response range is similar to that measured
467 experimentally in a saltmarsh species in an equivalent climate zone (e.g. Georgia,
468 (Giurgevich and Dunn, 1981)) and to the values hypothesised for the habitat from data
469 collected along the US Atlantic Coast, (Feher et al., 2017). The long-term average maximum
470 daytime temperature at this site is 19.2°C , which is cooler than the optimal range for NEE
471 suggesting temperature can be a significant limiting factor to productivity, especially during
472 the dormancy period where average monthly maximum temperatures are only 13.7°C to
473 16.6°C (Bureau of Meteorology). During the growing season the average maximum
474 temperatures are within the range of optimal NEE (20.6°C to 23.1°C), although hot days
475 ($>30^{\circ}\text{C}$) significantly depress NEE and depending on the year, can be common during
476 summer months (averaging 2-6 days per month). Within the diversity of saltmarsh species
477 found globally, some species have C4 photosynthetic pathways (Drake, 1989). C4
478 photosynthesis plants often exhibit higher optimum temperature ranges (30 - 35°C , Berry and
479 Björkman, 1980) than C3 photosynthesis plants (20 - 25), and the cooler conditions at this site
480 could explain the absence of C4 plants from this bioregion. The parabolic relationship
481 between NEP and air temperature and NEP and VPD suggest that higher air temperatures and
482 VPD (which are expected with climate change) could negatively impact CO_2 uptake by these
483 coastal ecosystems. High VPD was related to lower NEP, and to a lesser extent, lower ET
484 (Fig. 6d). However, VPD increases atmospheric demand for water, increasing the evaporation
485 from the saturated marsh surfaces in the footprint, and this atmospheric demand could be
486 forcing ET at high VPD rather than plant moderation via reduced transpiration, even if
487 transpiration is reduced. Thus, despite maintained ET during VPD periods we cannot
488 conclude a non-closure of stomata. NEP also reduced below a VPD of 1.92 KPa , but at our
489 field site low VPD correlated with low temperatures ($r = 0.88$), and low temperatures were
490 shown to limit NEP.

491

492 In saltmarshes, evapotranspiration occurs from plant mediated transpiration but also from soil
493 pores (which tend to be saturated), wetted leaves and open water. We observed average
494 evaporation rates of 2.48 mm day⁻¹ during the growing season and 0.97 mm day⁻¹ during the
495 dormant season. Actual evapotranspiration in this region modelled using the CMRSET
496 algorithm is estimated to range between 0.6 and 3.2 mm day⁻¹ during winter and summer
497 respectively (McVicar et al., 2022); our field measurements support the model. Overall,
498 rainfall is in excess of the requirements for maintaining ET at this site, although deficits can
499 develop for short periods during the growing season, when ET is higher, perhaps explaining
500 the drier saltmarsh surface during this period. Conversely, long term rainfall excess could be
501 contributing to the complicated hydrology at this location, where inundation is not strictly
502 associated with tidal stage (data not shown) and our observation of long (5-day) periods of
503 inundation during winter.

504

505 Growing season ET rates are significantly higher than those of the dormant season, partly due
506 to the solar configuration in winter as opposed to summer, but also due to phenological
507 changes. A big leaf model estimation of evapotranspiration from saltmarshes in New South
508 Wales estimates ET to be highly sensitive to vegetation height, increasing by more than 1 mm
509 day⁻¹ as vegetation height increases from 0.1 to 0.4 m (Hughes et al., 2001) and transpiration
510 in saltmarsh plants in the cold season has been shown to account for only 20% of the annual
511 transpiration budget (Giurgevich and Dunn, 1981) following the same pattern as the seasonal
512 distribution of productivity.

513

514 The rate of carbon uptake per unit of water loss (WUE) is a key ecosystem characteristic,
515 which is a result of a suite of physical and canopy physiological forcings, and has direct
516 implications for ecosystem function and global water and carbon cycling. Mean water use
517 efficiency (WUEe) of this saltmarsh was estimated at 0.86 g C kg⁻¹ H₂O, which is markedly
518 lower than for grass dominated saltmarshes in China (2.9 g C kg⁻¹ H₂O, Xiao et al. (2013))
519 but similar to the value for WUEe based on NEP and ET in mangroves (0.77 g C kg⁻¹ H₂O,
520 Krauss et al. (2022)), which are also C3 plants. The Chinese saltmarshes studied in Xiao et al.
521 (2013) are dominated by *Spartina alterniflora*, a C4 perennial grass. C4 plants have higher
522 (often double) water use efficiencies than C3 plants due to CO₂ concentrating mechanisms
523 (Osborne and Freckleton, 2009). The saltmarsh at French Island includes only C3 plants, and
524 the dominant chenopod *Sarcocornia quinqueflora* has been suspected to have higher
525 evapotranspiration rates than saltmarsh by approx. 15% (Hughes et al., 2001), but while

526 *Sarcocornia quinqueflora* dominates at this site, the footprint is a mix of species, and the
527 lower WUEe cannot be directly linked to the presence of *Sarcocornia quinqueflora*.
528 Furthermore, like most wetlands, the wetland surface is a mixed composition of emergent
529 vegetation, unsaturated soil and water bodies thus the spatial scale at which WUEe is
530 determined encompasses both the canopy (E_c) as well as any open water present in the
531 footprint. Transpiration is predicted to account for only 55% of ET in these systems (Hughes
532 et al., 2001), which is an E_c to ET ratio similar to that of mangroves (Krauss et al., 2022) but
533 significantly lower than terrestrial forests where more than 90% of ET can be attributed to
534 transpiration. Thus, regional variations in WUEe can be attributed to multiple forcings that
535 form complex spatiotemporal patterns.

536

537 Saltmarshes are considered among the most productive ecosystems on Earth with an
538 estimated global NEP of 634 Tg C y^{-1} (Fagherazzi et al., 2013) and 601 634 Tg C y^{-1}
539 (Rosentreter et al., 2023). Productivity of southern Australian marshes was previously
540 estimated at 0.8 kg $m^{-2} y^{-1}$ by repeated measurements of above ground standing crops (Clarke
541 and Jacoby, 1994), which if not accounting for season, equates to 2.2 g C $m^{-2} d^{-1}$. Similar
542 studies on saltmarshes in France report lower productivity (483 g C $m^{-2} y^{-1}$, (Mayen et al.,
543 2024)) and daily growing season rates of 1.53 g C $m^{-2} d^{-1}$, but mid-latitude saltmarsh sites in
544 the USA and China show productivity rates of 775 g C $m^{-2} y^{-1}$, (Wang et al., 2016) and 668 g
545 C $m^{-2} y^{-1}$, (Xiao et al., 2013) respectively. It is clear that productivity across climate zones
546 and biogeographic regions varies widely with some studies even reporting net emissions over
547 an annual period from some marshes and a global average estimated between 382 (Alongi,
548 2020) and 1,585 g C $m^{-2} y^{-1}$ (Chmura et al., 2003), albeit based on a small subset of studies.
549 An analysis of GPP across latitudes in the USA show that warmer sites (including mangrove
550 wetlands in southern USA) had significantly higher GPP than mid-latitude saltmarshes such
551 as the one on French Island (Feagin et al., 2020). Mangroves have higher NEE than
552 saltmarshes, estimated by Krauss et al. (2022) to average 1200 g C $m^{-2} y^{-1}$. While our data
553 does not provide enough coverage for a long-term annual estimate of carbon flux, our daily
554 values of an average of 2.88 g C $m^{-2} d^{-1}$ during the growing season, combined with the
555 relatively short dormant season relative to other temperate locations, suggest a high carbon
556 sequestration rate for this ecosystem type. In another southern hemisphere study, growing
557 season rates at an EC tower site in Argentina, are extrapolated by us to average 1.6 g C $m^{-2} d^{-1}$
558 (Bautista et al., 2023) but in that saltmarsh, flooding reduced vegetation biomass and
559 productivity.

560

561 The data presented here is the exchange of carbon between the land surface and the
562 atmosphere, but saltmarshes, like other marine connected communities, exchange carbon also
563 through dissolved carbon pathways, which can be significant (Cai, 2011). Thus, the fluxes
564 presented here do not constitute the entire carbon budget of this ecosystem.

565

566 5. Conclusions

567

568 The response of the French Island saltmarsh to environmental drivers is indicative of the
569 complex interactions determining saltmarsh productivity. The unique long-term, high-
570 resolution record enabled us to derive temperature, VPD and light response functions, thus
571 formulating equations that describe how climate-change sensitive parameters such as
572 temperature, relative humidity, and cloud cover, affect CO₂ uptake, respiration and
573 evapotranspiration. The marsh operated as a CO₂ sink throughout the various canopy
574 phenological phases, but during the dormant period, CO₂ uptake was less than 25% that of
575 the growing season. Seasonality of greenhouse gas fluxes in Australian saltmarshes is an
576 understudied but important aspect of global carbon budgeting.

577

578 Competing interests

579

580 The contact author has declared that none of the authors has any competing interests.

581

582 Acknowledgments

583

584 The work was carried out with the permission of Parks Victoria (Permit 10008684). We thank
585 Phil and Yuko Bock for logistic support and accommodation on French Island. We thank
586 Leigh Burgess, Kiri Mason and Ian McHugh for technical support and the Australian OzFlux
587 community for ongoing collaboration. This work was funded by an Australian Research
588 Council Discovery Award to RR and ED (DP220102873) as well as a Monash University
589 Networks of Excellence award to RR.

590

591 Data Availability

592 Data used for this analysis is available at <https://figshare.com/s/ba62aafd1a4049248a08> (note
593 that this is a temporary private link to an embargoed dataset which will be replaced with a
594 publicly available DOI upon publication).

595

596 Author contribution

597 RR conceptualised the study, acquired funding, prepared the manuscript, designed and
598 carried out the field campaign, and performed the analysis. ED acquired funding, developed
599 methodology and prepared the manuscript. AG developed methodology and prepared the
600 manuscript. TA, EJVH, HR and MP were involved in the field investigation and
601 administration of the project and provided edits on the manuscript.

602

603 References

604

605 Adam, P.: Saltmarsh Ecology, Cambridge University Press, 1990.

606 Adam, P.: Morecambe Bay saltmarshes: 25 years of change, in: British Saltmarshes, Forrest
607 Text, Cardigan, UK, 81–107, 2000.

608 Adam, P.: Saltmarshes in a time of change, *Environ. Conserv.*, 29, 39–61,
609 <https://doi.org/10.1017/S0376892902000048>, 2002.

610 Alongi, D. M.: Carbon balance in salt marsh and mangrove ecosystems: A global synthesis, *J.*
611 *Mar. Sci. Eng.*, 8, 767, 2020.

612 Artigas, F., Shin, J. Y., Hobbie, C., Marti-Donati, A., Schäfer, K. V. R., and Pechmann, I.:
613 Long term carbon storage potential and CO₂ sink strength of a restored salt marsh in New
614 Jersey, *Agric. For. Meteorol.*, 200, 313–321, <https://doi.org/10.1016/j.agrformet.2014.09.012>,
615 2015.

616 Baldocchi, D. D.: Assessing the eddy covariance technique for evaluating carbon dioxide
617 exchange rates of ecosystems: past, present and future, *Glob. Change Biol.*, 9, 479–492,
618 <https://doi.org/10.1046/j.1365-2486.2003.00629.x>, 2003.

619 Bautista, N. E., Gassmann, M. I. , and Pérez, C. F.: Gross primary production, ecosystem
620 respiration, and net ecosystem production in a southeastern South American salt marsh.
621 *Estuaries Coast*, 46, 1923–1937, <https://doi.org/10.1007/s12237-023-01224-8>, 2023.

622

623 Berry, J., and Björkman, O.: Photosynthetic response and adaptation to temperature in higher
624 plants, *Ann. Rev. Plant Physiol.*, 31, 491–543,
625 <https://doi.org/10.1146/annurev.pp.31.060180.002423>, 1980.

626

627 Borges, A. V., Schiettecatte, L.-S., Abril, G., Delille, B., and Gazeau, F.: Carbon dioxide in
628 European coastal waters, *Trace Gases Eur. Coast. Zone*, 70, 375–387,
629 <https://doi.org/10.1016/j.ecss.2006.05.046>, 2006.

- 630 Cai, W.-J.: Estuarine and coastal ocean carbon paradox: CO₂ sinks or sites of terrestrial
631 carbon incineration?, *Annu. Rev. Mar. Sci.*, 3, 123–145, [https://doi.org/10.1146/annurev-](https://doi.org/10.1146/annurev-marine-120709-142723)
632 [marine-120709-142723](https://doi.org/10.1146/annurev-marine-120709-142723), 2011.
- 633 Chen, J., Falk, M., Euskirchen, E., Paw U, K. T., Suchanek, T. H., Ustin, S. L., Bond, B. J.,
634 Brosofske, K. D., Phillips, N., and Bi, R.: Biophysical controls of carbon flows in three
635 successional Douglas-fir stands based on eddy-covariance measurements, *Tree Physiol.*, 22,
636 169–177, <https://doi.org/10.1093/treephys/22.2-3.169>, 2002.
- 637 Chmura, G. L., Anisfeld, S. C., Cahoon, D. R., and Lynch, J. C.: Global carbon sequestration
638 in tidal, saline wetland soils, *Glob. Biogeochem. Cycles*, 17,
639 <https://doi.org/10.1029/2002GB001917>, 2003.
- 640 Clarke, P., J. and Jacoby, C. A.: Biomass and above-ground productivity of salt-marsh plants
641 in South-eastern Australia, *Aust. J. Mar. Freshw. Res.*, 45, 1521–1528, 1994.
- 642 Davis, K. J., Bakwin, P. S., Yi, C., Berger, B. W., Zhao, C., Teclaw, R. M., and Isebrands, J.
643 G.: The annual cycles of CO₂ and H₂O exchange over a northern mixed forest as observed
644 from a very tall tower, *Glob. Change Biol.*, 9, 1241–1332, [https://doi.org/10.1046/j.1365-](https://doi.org/10.1046/j.1365-2486.2003.00672.x)
645 [2486.2003.00672.x](https://doi.org/10.1046/j.1365-2486.2003.00672.x), 2003.
- 646 Drake, B. G.: Photosynthesis of salt marsh species, *Aquat. Bot.*, 34, 167–180,
647 [https://doi.org/10.1016/0304-3770\(89\)90055-7](https://doi.org/10.1016/0304-3770(89)90055-7), 1989.
- 648
649 Duarte, C. M.: Reviews and syntheses: Hidden forests, the role of vegetated coastal habitats
650 in the ocean carbon budget, *Biogeosciences*, 14, 301–310, [https://doi.org/10.5194/bg-14-301-](https://doi.org/10.5194/bg-14-301-2017)
651 [2017](https://doi.org/10.5194/bg-14-301-2017), 2017.
- 652 Erickson, J. E., Peresta, G., Montovan, K. J., and Drake, B. G.: Direct and indirect effects of
653 elevated atmospheric CO₂ on net ecosystem production in a Chesapeake Bay tidal wetland,
654 *Glob. Change Biol.*, 19, 3368–3378, 2013.
- 655 Fagherazzi, S., Wiberg, P. L., Temmerman, S., Struyf, E., Zhao, Y., and Raymond, P. A.:
656 Fluxes of water, sediments, and biogeochemical compounds in salt marshes, *Ecol. Process.*,
657 2, 3, <https://doi.org/10.1186/2192-1709-2-3>, 2013.
- 658 Feagin, R. A., Forbrich, I., Huff, T. P., Barr, J. G., Ruiz-Plancarte, J., Fuentes, J. D., Najjar,
659 R. G., Vargas, R., Vázquez-Lule, A., Windham-Myers, L., Kroeger, K. D., Ward, E. J.,
660 Moore, G. W., Leclerc, M., Krauss, K. W., Stagg, C. L., Alber, M., Knox, S. H., Schäfer, K.
661 V. R., Bianchi, T. S., Hutchings, J. A., Nahrawi, H., Noormets, A., Mitra, B., Jaimes, A.,
662 Hinson, A. L., Bergamaschi, B., King, J. S., and Miao, G.: Tidal wetland gross primary
663 production across the continental United States, 2000–2019, *Glob. Biogeochem. Cycles*, 34,
664 [e2019GB006349](https://doi.org/10.1029/2019GB006349), <https://doi.org/10.1029/2019GB006349>, 2020.
- 665 Feher, L. C., Osland, M. J., Griffith, K. T., Grace, J. B., Howard, R. J., Stagg, C. L.,
666 Enwright, N. M., Krauss, K. W., Gabler, C. A., Day, R. H., and Rogers, K.: Linear and
667 nonlinear effects of temperature and precipitation on ecosystem properties in tidal saline
668 wetlands, *Ecosphere*, 8, e01956, <https://doi.org/10.1002/ecs2.1956>, 2017.

- 669 Gedan, K. B., Silliman, B. R., and Bertness, M. D.: Centuries of human-driven change in salt
670 marsh ecosystems, *Annu. Rev. Mar. Sci.*, 1, 117–141,
671 <https://doi.org/10.1146/annurev.marine.010908.163930>, 2009.
- 672 Ghosh, S. and Mishra, D. R.: Analyzing the long-term phenological trends of salt marsh
673 ecosystem across coastal Louisiana, *Remote Sens.*, 9, <https://doi.org/10.3390/rs9121340>,
674 2017.
- 675 Giurgevich, J. R. and Dunn, E. L.: A comparative analysis of the CO₂ and water vapor
676 responses of two *Spartina* species from Georgia coastal marshes, *Estuar. Coast. Shelf Sci.*,
677 12, 561–568, [https://doi.org/10.1016/S0302-3524\(81\)80082-5](https://doi.org/10.1016/S0302-3524(81)80082-5), 1981.
- 678 Hilker, T., Hall, F. G., Coops, N. C., Lyapustin, A., Wang, Y., Nesic, Z., Grant, N., Black, T.
679 A., Wulder, M. A., Kljun, N., Hopkinson, C., and Chasmer, L.: Remote sensing of
680 photosynthetic light-use efficiency across two forested biomes: Spatial scaling, *Remote Sens.*
681 *Environ.*, 114, 2863–2874, <https://doi.org/10.1016/j.rse.2010.07.004>, 2010.
- 682 Hill, A. C. and Vargas, R.: Methane and carbon dioxide fluxes in a temperate tidal salt marsh:
683 comparisons between plot and ecosystem measurements, *J. Geophys. Res. Biogeosciences*,
684 127, e2022JG006943, <https://doi.org/10.1029/2022JG006943>, 2022.
- 685 Howe, A. J., Rodríguez, J. F., Spencer, J., MacFarlane, G. R., and Saintilan, N.: Response of
686 estuarine wetlands to reinstatement of tidal flows, *Mar. Freshw. Res.*, 61, 702–713, 2010.
- 687 Hughes, C. E., Kalma, J. D., Binning, P., Willgoose, G. R., and Vertzonis, M.: Estimating
688 evapotranspiration for a temperate salt marsh, Newcastle, Australia, *Hydrol. Process.*, 15,
689 957–975, <https://doi.org/10.1002/hyp.189>, 2001.
- 690 Huxham, M., Whitlock, D., Githaiga, M., and Dencer-Brown, A.: Carbon in the coastal
691 seascape: how interactions between mangrove forests, seagrass meadows and tidal marshes
692 influence carbon storage, *Curr. For. Rep.*, 4, 101–110, <https://doi.org/10.1007/s40725-018-0077-4>, 2018.
- 694 Kathilankal, J. C., Mozdzer, T. J., Fuentes, J. D., D’Odorico, P., McGlathery, K. J., and
695 Zieman, J. C.: Tidal influences on carbon assimilation by a salt marsh, *Environ. Res. Lett.*, 3,
696 044010, <https://doi.org/10.1088/1748-9326/3/4/044010>, 2008.
- 697 Kljun, N., Calanca, P., Rotach, M. W., and Schmid, H. P.: A simple two-dimensional
698 parameterisation for Flux Footprint Prediction (FFP), *Geosci Model Dev*, 8, 3695–3713,
699 <https://doi.org/10.5194/gmd-8-3695-2015>, 2015.
- 700 Krauss, K. W., Lovelock, C. E., Chen, L., Berger, U., Ball, M. C., Reef, R., Peters, R.,
701 Bowen, H., Vovides, A. G., Ward, E. J., and others: Mangroves provide blue carbon
702 ecological value at a low freshwater cost, *Sci. Rep.*, 12, <https://doi.org/10.1038/s41598-022-02041-x>, 2022.
- 703 Lasslop, G., Reichstein, M., Papale, D., Richardson, A. D., Arneeth, A., BARR, A., STOY, P.,
704 and WOHLFAHRT, G.: Separation of net ecosystem exchange into assimilation and
705 respiration using a light response curve approach: critical issues and global evaluation, *Glob.*
706 *Change Biol.*, 16, 187–208, <https://doi.org/10.1111/j.1365-2486.2009.02041.x>, 2010.

- 707 Lu, W., Xiao, J., Liu, F., Zhang, Y., Liu, C., and Lin, G.: Contrasting ecosystem CO₂ fluxes
708 of inland and coastal wetlands: a meta-analysis of eddy covariance data, *Glob. Change Biol.*,
709 23, 1180–1198, <https://doi.org/10.1111/gcb.13424>, 2017.
- 710 Mayen, J., Polsenaere, P., Lamaud, É., Arnaud, M., Kostyrka, P., Bonnefond, J.-M., Geairon,
711 P., Gernigon, J., Chassagne, R., and Lacoue-Labarthe, T.: Atmospheric CO₂ exchanges
712 measured by eddy covariance over a temperate salt marsh and influence of environmental
713 controlling factors, *Biogeosciences*, 21, 993–1016, 2024.
- 714 McLeod, E., Chmura, G. L., Bouillon, S., Salm, R., Björk, M., Duarte, C. M., Lovelock, C.
715 E., Schlesinger, W. H., and Silliman, B. R.: A blueprint for blue carbon: toward an improved
716 understanding of the role of vegetated coastal habitats in sequestering CO₂, *Front. Ecol.*
717 *Environ.*, 9, 552–560, <https://doi.org/10.1890/110004>, 2011.
- 718 Mcowen, C. J., Weatherdon, L. V., Bochove, J.-W. V., Sullivan, E., Blyth, S., Zockler, C.,
719 Stanwell-Smith, D., Kingston, N., Martin, C. S., Spalding, M., and Fletcher, S.: A global map
720 of saltmarshes, *Biodivers. Data J.*, 5, e11764, <https://doi.org/10.3897/BDJ.5.e11764>, 2017.
- 721 McVicar, T., Vleeshouwer, J., Van Niel, T., Guerschman, J., and Peña-Arancibia, J. L.:
722 Actual Evapotranspiration for Australia using CMRSET algorithm. Version 1.0, 2022.
- 723 Mitsch, W. J. and Gosselink, J. G.: The value of wetlands: importance of scale and landscape
724 setting, *Ecol. Econ.*, 35, 25–33, [https://doi.org/10.1016/S0921-8009\(00\)00165-8](https://doi.org/10.1016/S0921-8009(00)00165-8), 2000.
- 725 Moffett, K. B., Wolf, A., Berry, J. A., and Gorelick, S. M.: Salt marsh–atmosphere exchange
726 of energy, water vapor, and carbon dioxide: Effects of tidal flooding and biophysical controls,
727 *Water Resour. Res.*, 46, 2010.
- 728 Nahrawi, H., Leclerc, M. Y., Pennings, S., Zhang, G., Singh, N., and Pahari, R.: Impact of
729 tidal inundation on the net ecosystem exchange in daytime conditions in a salt marsh, *Agric.*
730 *For. Meteorol.*, 294, 108133, <https://doi.org/10.1016/j.agrformet.2020.108133>, 2020.
- 731 Navarro, A., Young, M., Macreadie, P. I., Nicholson, E., and Ierodiaconou, D.: Mangrove
732 and saltmarsh distribution mapping and land cover change assessment for south-eastern
733 Australia from 1991 to 2015, *Remote Sens.*, 13, <https://doi.org/10.3390/rs13081450>, 2021.
- 734 Osborne, C. P. and Freckleton, R. P.: Ecological selection pressures for C4 photosynthesis in
735 the grasses. *Proc. Roc. Soc. B*, 276, <https://doi.org/10.1098/rspb.2008.1762>, 2009.
- 736 Otani, S. and Endo, T.: CO₂ flux in tidal flats and salt marshes, *Blue Carbon Shallow Coast.*
737 *Ecosyst. Carbon Dyn. Policy Implement.*, 223–250, 2019.
- 738 Owers, C. J., Rogers, K. and Woodroffe, C. D.: Spatial variation of above-ground carbon
739 storage in temperate coastal wetlands. *Estuar. Coast. Shelf Sci.*, 210, 55-67,
740 <https://doi.org/10.1016/j.ecss.2018.06.002>, 2018
- 741
742 R Core Team: R: A Language Environment for Statistical Computing. Vienna, Australia,
743 2024.
- 744 Reents, S., Möller, I., Evans, B. R., Schoutens, K., Jensen, K., Paul, M., Bouma, T. J.,
745 Temmerman, S., Lustig, J., Kudella, M., and Nolte, S.: Species-specific and seasonal

- 746 differences in the resistance of salt-marsh vegetation to wave impact, *Front. Mar. Sci.*, 9,
747 2022.
- 748 Rosentreter, J. A., Laruelle, G. G., Bange, H. W., Bianchi, T. S., Busecke, J. J. M., Cai, W. J.,
749 Eyre, B. D., Forbich, I., Kwon, E. Y., Maavara, T., Moosdorf, N., Najjar, R. G., Sarma, V. V.
750 S. S., Van Dam, B. and Regnier, P.: Coastal vegetation and estuaries are collectively a
751 greenhouse gas sink. *Nat. Clim. Chang.* 13, 579–587. [https://doi.org/10.1038/s41558-023-](https://doi.org/10.1038/s41558-023-01682-9)
752 [01682-9](https://doi.org/10.1038/s41558-023-01682-9), 2023.
- 753
- 754 Schäfer, K. V. R., Duman, T., Tomasicchio, K., Tripathee, R., and Sturtevant, C.: Carbon
755 dioxide fluxes of temperate urban wetlands with different restoration history, *Agric. For.*
756 *Meteorol.*, 275, 223–232, <https://doi.org/10.1016/j.agrformet.2019.05.026>, 2019.
- 757 Seyfferth, A. L., Bothfeld, F., Vargas, R., Stuckey, J. W., Wang, J., Kearns, K., Michael, H.
758 A., Guimond, J., Yu, X., and Sparks, D. L.: Spatial and temporal heterogeneity of
759 geochemical controls on carbon cycling in a tidal salt marsh, *Geochim. Cosmochim. Acta*,
760 282, 1–18, 2020.
- 761 Shepard, C. C., Crain, C. M., and Beck, M. W.: The protective role of coastal marshes: a
762 systematic review and meta-analysis, *PLoS ONE*, 6, e27374,
763 <https://doi.org/10.1371/journal.pone.0027374>, 2011.
- 764 Smith, J. A. M., Regan, K., Cooper, N. W., Johnson, L., Olson, E., Green, A., Tash, J., Evers,
765 D. C., and Marra, P. P.: A green wave of saltmarsh productivity predicts the timing of the
766 annual cycle in a long-distance migratory shorebird, *Sci. Rep.*, 10, 20658,
767 <https://doi.org/10.1038/s41598-020-77784-7>, 2020.
- 768 Vázquez-Lule, A. and Vargas, R.: Biophysical drivers of net ecosystem and methane
769 exchange across phenological phases in a tidal salt marsh, *Agric. For. Meteorol.*, 300,
770 108309, <https://doi.org/10.1016/j.agrformet.2020.108309>, 2021.
- 771 Wang, Z. A., Kroeger, K. D., Ganju, N. K., Gonneea, M. E., and Chu, S. N.: Intertidal salt
772 marshes as an important source of inorganic carbon to the coastal ocean, *Limnol. Oceanogr.*,
773 61, 1916–1931, <https://doi.org/10.1002/lno.10347>, 2016.
- 774 Ward, N. D., Megonigal, J. P., Bond-Lamberty, B., Bailey, V. L., Butman, D., Canuel, E. A.,
775 Diefenderfer, H., Ganju, N. K., Goñi, M. A., and Graham, E. B.: Representing the function
776 and sensitivity of coastal interfaces in Earth system models, *Nat. Commun.*, 11, 2458, 2020.
- 777 Wei, S., Han, G., Jia, X., Song, W., Chu, X., He, W., Xia, J., and Wu, H.: Tidal effects on
778 ecosystem CO₂ exchange at multiple timescales in a salt marsh in the Yellow River Delta,
779 *Estuar. Coast. Shelf Sci.*, 238, 106727, 2020.
- 780 Whitfield, A. K.: The role of seagrass meadows, mangrove forests, salt marshes and reed
781 beds as nursery areas and food sources for fishes in estuaries, *Rev. Fish Biol. Fish.*, 27, 75–
782 110, <https://doi.org/10.1007/s11160-016-9454-x>, 2017.
- 783 Xiao, J., Sun, G., Chen, J., Chen, H., Chen, S., Dong, G., Gao, S., Guo, H., Guo, J., Han, S.,
784 Kato, T., Li, Y., Lin, G., Lu, W., Ma, M., McNulty, S., Shao, C., Wang, X., Xie, X., Zhang,
785 X., Zhang, Z., Zhao, B., Zhou, G., and Zhou, J.: Carbon fluxes, evapotranspiration, and water

786 use efficiency of terrestrial ecosystems in China, *Agric. For. Meteorol.*, 182–183, 76–90,
787 <https://doi.org/10.1016/j.agrformet.2013.08.007>, 2013.

788